367-06-006 ISMRM ABSTRACT

Choice of IVIM-DWI fitting substantially impacts parameter estimation in multi-center renal studies

Digital Poster · 55 min View Poster | Advanced Methods in Renal MRI · Session: 5:05–6:00 PM · Digital Posters Row H · 6 **Keywords:**
DIFFUSION ANALYSIS AND VISUALIZATION IVIM-DWI MULTI-CENTRE RENAL MULTI-VENDOR

Siria Pasini [1], **Rebeca Echeverria-Chasco** [2], **Leyre Garcia-Ruiz** [2], **Steffen Ringgaard** [3], **Oliver J Gurney-Champion** [4], **Ivan A Rashid** [5], **Anika Strittmatter** [6,7], **GIULIA VILLA** [1], **Anish Raj** [6,7], **Ioana Urdea** [8], **Susan Francis** [9], **Christoffer Laustsen** [3], **Frank G Zoellner** [6,7], **Maria Fernandez-Seara** [2], **Anna Caroli** [1]

[1]Istituto di Ricerche Farmacologiche Mario Negri IRCCS, Ranica (BG), Italy
[2]Department of Radiology, Clinica Universidad de Navarra, Pamplona, Spain
[3]MR Research Centre, Aarhus University, Aarhus, Denmark
[4]Department of Radiology and Nuclear Medicine, Amsterdam University Medical Center, University of Amsterdam, Amsterdam, Netherlands
[5]Medical Radiation Physics, Department of Translational Medicine, Lund University, Lund, Sweden
[6]Computer Assisted Clinical Medicine, Medical Faculty Mannheim, Heidelberg University, Mannheim, Germany
[7]Mannheim Institute for Intelligent Systems in Medicine, Medical Faculty Mannheim, Heidelberg University, Mannheim, Germany
[8]Siemens, Brasov, Romania
[9]Sir Peter Mansfield Imaging Centre, University of Nottingham, Nottingham, United Kingdom

Presenting Author: *Siria Pasini (siria.pasini@marionegri.it)*

Impact

Renal IVIM-DWI parameter estimates depend strongly on fitting algorithm, with different best-performing algorithms across sites, despite protocol standardization. Reliable algorithm selection and site-specific performance assessment are essential for reproducible multi-center studies and quantitative renal imaging clinical translation.

Synopsis

Motivation: Renal IVIM-DWI provides non-invasive assessment of renal microstructure and perfusion, however parameter reliability is limited by differences in fitting algorithms. Evaluating algorithm impact is fundamental for consistent parameter estimation in multi-center studies.

Goals: To evaluate the dependence of renal IVIM-DWI parameters on fitting algorithm and identify the best-performing approaches across sites using harmonized acquisition protocols.

Approach: Multi-center 3T DWI data from healthy volunteers were processed using open-source, tested, harmonized codes. Algorithms performance was assessed using error metrics, parameter variability, and clustering analysis.

Results: Algorithm selection substantially impacted parameter estimation. Algorithm 9 (full biexponential fit) performed best globally, and D showed the highest stability.

Introduction

Intravoxel Incoherent Motion (IVIM) diffusion-weighted imaging (DWI)[1] has emerged as a promising technique in renal studies to non-invasively probe renal pathophysiology, with potential applications in prognosis and patient stratification[2–4]. However, IVIM parameter estimates are often limited by low reliability and noisy parameter maps[5], and cross-study comparisons are frequently hindered by methodological differences in acquisition protocols and post-processing strategies[6,7]. The aim of this preliminary study was to assess the dependence of renal IVIM-DWI parameters on IVIM fitting algorithms and to identify the best-performing subset of algorithms, using multi-center data acquired with harmonised protocols.

Methods

Healthy volunteers (HV) from the RESPECT clinical study (clinicaltrials.gov ID NCT05229263) were enrolled at four sites (Aarhus University, Denmark-AUH; Heidelberg University, Germany-UHEI; Clinical University of Navarra, Spain-UNAV; Istituto di Ricerche Farmacologiche Mario Negri IRCCS, Italy-IRFMN). MRI examinations were performed on 3T systems from two different vendors, with body phased-array receiver coils. DWI data were acquired following a standardized protocol developed by UKRIN-MAPS[8,9] (Fig.1) using an echo-planar imaging sequence with 13 b-values (0, 5–800s/mm²) applied along six gradient directions. At UHEI, due to scanner restrictions, a reduced set of 7 b-values (0, 50–800s/mm²) was collected. DWI data were pseudonymised and pre-processed including distortion correction using FSL "topup"[10](b0-pairs with reversed phase encoding), denoising and between-volumes motion correction via "dipy" library[11]. Motion-corrected data were then coregistered to T1-weighted and T2-weighted anatomical images and transformations were applied to final parameter maps. Whole kidneys, cortical and medullary masks were outlined on T1-weighted images using an in-house deep-learning-based segmentation tool manually corrected in ITK-SNAP[12]. For each site, five HVs with minimal motion across b-values were selected for subsequent analysis. IVIM parameters, pure diffusion (D), pseudodiffusion (D*) and perfusion fraction (F), were estimated using the open-source standardized algorithms provided by OSIPI repository[13] (Fig.1) with a threshold[14] for segmented approaches at 200s/mm². IVIM fitting models were compared to evaluate their performance and parameter variability based on: (i)signal-to-model root mean square error (RMSE), (ii)Akaike Information Criterion (AIC)[15], (iii)proportion of non-physical parameter values, (iv)median parameter value outside the interquartile range (IQR), and (v)parameter variability across slices (CV%). For each volunteer, K-means clustering grouped algorithms with similar performance metrics[16]. Algorithms were ranked per site by average z-score, and the best-performing ones, consistently in the lowest-z cluster, were identified across sites. Intraclass correlation coefficients (ICC(2,1))[17] quantified parameter reliability, and linear mixed-effects models partitioned variance into participant- and algorithm-related components.

Results

Representative IVIM parameter maps for each algorithm are shown in Fig.2, and individual HV analyses in Fig.3. Algorithm 16 consistently yielded the highest percentage of non-physical values (>80%) and the largest intra-slice coefficient of variation (>70%). Algorithms with the lowest percentage of non-physical values varied by site but remained below 2.5% and the lowest intra-slice CV was consistently observed for Algorithm 15. Across all algorithms, D* exhibited the greatest variability, while D was the most stable. For outliers, Algorithm 2 consistently showed values within the overall interquartile range (IQR), with no outliers detected, whereas Algorithms 1 and 13 displayed the highest number of outliers. Furthermore, Algorithm 13 exhibited the largest AIC and RMSE values across sites using the full protocol (AUH, IRFMN, and UNAV). Cluster analysis (Fig.4) identified thirteen algorithms that consistently achieved top-cluster performance. The best-performing algorithms were 2, 8, 9, and 9 for UHEI, UNAV, AUH, and IRFMN respectively, with 9 confirmed globally. ICC results (Fig.5) demonstrated moderate to good reliability for D across best-performing algorithms and sites. Across parameters, participant variability accounted for the majority of total variance.

Discussion

This multi-center and multi-vendor study investigated IVIM parameters dependence on fitting algorithm, using renal DWI data acquired with standardized protocol and processed with 20 open-source, fully tested, harmonized codes from the OSIPI repository. For all algorithms, D exhibited the lowest variability while D* showed the greatest variability. The best-performing fits were consistently obtained using the full biexponential model (9,8,2), followed by segmented fitting approaches (5,6). Interestingly, for the two sites with the same vendor and protocol, the same algorithm was identified as best-performing. A limitation of this study is the relatively small sample size, with only 20 healthy volunteers. Future studies on larger cohorts and repeated acquisitions are needed to confirm current results and better characterize inter-session variability.

Conclusion

This study demonstrates that the choice of IVIM fitting algorithm substantially impacts parameter estimation, highlighting the need to assess algorithms performance on in-vivo multi-center before clinical application. For this preliminary study on renal multicenter dataset, Algorithm 9, employing a full biexponential fit, was the best-performing globally. Among renal IVIM parameters, D exhibited the highest stability across algorithms.

Acknowledgements

Acknowledgments: This study was supported by the Italian Ministry of Health, Gobierno de Navarra, German Federal Ministry of Research, Technology and Space (BMFTR, grant number 01KU2102 and 01KU2504), and Innovation Fund Denmark (IFD), under the frame of ERA PerMed (ERAPerMed-2020-326) and EPPerMed (EPPERMED2024-168).

References

1. Le Bihan, D.; Breton, E.; Lallemand, D.; Aubin, M. L.; Vignaud, J.; Laval-Jeantet, M. Separation of Diffusion and Perfusion in Intravoxel Incoherent Motion MR Imaging. Radiology 1988, 168 (2), 497–505. https://doi.org/10.1148/radiology.168.2.3393671.

2. Yu, Y.; Zhang, W.; Zhu, L.; Zhou, H.; Liang, S.; Zhang, L.; Liu, Z.; Zhang, J. Utility of the Combination of IVIM-DWI MRI and Baseline eGFR for Identifying a High Risk of Chronic Kidney Disease Progression. Front. Med. 2025, 12, 1532210. https://doi.org/10.3389/fmed.2025.1532210.

3. Bodard, S.; Cornelis, F. H. Non-Invasive Functional MRI Techniques for Early Detection of Kidney Injury in Chronic Kidney Disease: A Positive Step Forward. Ann Transl Med 2024, 12 (4), 80–80. https://doi.org/10.21037/atm-23-1788.

4. Cox, E. F.; Buchanan, C. E.; Bradley, C. R.; Prestwich, B.; Mahmoud, H.; Taal, M.; Selby, N. M.; Francis, S. T. Multiparametric Renal Magnetic Resonance Imaging: Validation, Interventions, and Alterations in Chronic Kidney Disease. Front Physiol 2017, 8, 696. https://doi.org/10.3389/fphys.2017.00696.

5. Gurney-Champion, O. J.; Klaassen, R.; Froeling, M.; Barbieri, S.; Stoker, J.; Engelbrecht, M. R. W.; Wilmink, J. W.; Besselink, M. G.; Bel, A.; Van Laarhoven, H. W. M.; Nederveen, A. J. Comparison of Six Fit Algorithms for the Intra-Voxel Incoherent Motion Model of Diffusion-Weighted Magnetic Resonance Imaging Data of Pancreatic Cancer Patients. PLoS ONE 2018, 13 (4), e0194590. https://doi.org/10.1371/journal.pone.0194590.

6. Wang, X.; Ye, Z.; Li, S.; Yan, Z.; Cheng, J.; Ning, G.; Hou, Z. A Multicenter Study of Cervical Cancer Using Quantitative Diffusion-Weighted Imaging. Acta Radiol 2024, 65 (7), 851–859. https://doi.org/10.1177/02841851231222360.

7. Koh, D.-M.; Collins, D. J.; Orton, M. R. Intravoxel Incoherent Motion in Body Diffusion-Weighted MRI: Reality and Challenges. American Journal of Roentgenology 2011, 196 (6), 1351–1361. https://doi.org/10.2214/AJR.10.5515.

8. Buchanan, C.; Li, H.; Morris, D.; Daniel, A.; Sousa, J.; Sourbron, S.; Thomas, D.; Priest, A.; Francis, S. A Travelling Kidney Study Using a Harmonised Multiparametric Renal MRI Protocol; Joint Annual Meeting ISMRM-ESMRMB ISMRT 31st Annual Meeting, London, UK; p 0482. https://doi.org/10.58530/2022/0482.

9. Buchanan, C. E.; Li, H.; Nery, F.; Daniel, A. J.; Sousa, J. D.; Sourbron, S.; Priest, A.; Thomas, D.; Francis, T. Harmonisation of Multiparametric Renal MRI for Multi-Centre Studies; Proc. Intl. Soc. Mag. Reson. Med. 29, 2019.

10. Smith, S. M.; Jenkinson, M.; Woolrich, M. W.; Beckmann, C. F.; Behrens, T. E. J.; Johansen-Berg, H.; Bannister, P. R.; De Luca, M.; Drobnjak, I.; Flitney, D. E.; Niazy, R. K.; Saunders, J.; Vickers, J.; Zhang, Y.; De Stefano, N.; Brady, J. M.; Matthews, P. M. Advances in Functional and Structural MR Image Analysis and Implementation as FSL. NeuroImage 2004, 23, S208–S219. https://doi.org/10.1016/j.neuroimage.2004.07.051.

11. Garyfallidis, E.; Brett, M.; Amirbekian, B.; Rokem, A.; Van Der Walt, S.; Descoteaux, M.; Nimmo-Smith, I.; Dipy Contributors. Dipy, a Library for the Analysis of Diffusion MRI Data. Front. Neuroinform. 2014, 8. https://doi.org/10.3389/fninf.2014.00008.

12. Yushkevich, P. A.; Piven, J.; Hazlett, H. C.; Smith, R. G.; Ho, S.; Gee, J. C.; Gerig, G. User-Guided 3D Active Contour Segmentation of Anatomical Structures: Significantly Improved Efficiency and Reliability. NeuroImage 2006, 31 (3), 1116–1128. https://doi.org/10.1016/j.neuroimage.2006.01.015.

13. IVIM Code Collection. https://github.com/OSIPI/TF2.4_IVIM-MRI_CodeCollection.

14. Ljimani, A.; Caroli, A.; Laustsen, C.; Francis, S.; Mendichovszky, I. A.; Bane, O.; Nery, F.; Sharma, K.; Pohlmann, A.; Dekkers, I. A.; Vallee, J.-P.; Derlin, K.; Notohamiprodjo, M.; Lim, R. P.; Palmucci, S.; Serai, S. D.; Periquito, J.; Wang, Z. J.; Froeling, M.; Thoeny, H. C.; Prasad, P.; Schneider, M.; Niendorf, T.; Pullens, P.; Sourbron, S.; Sigmund, E. E. Consensus-Based Technical Recommendations for Clinical Translation of Renal Diffusion-Weighted MRI. Magn Reson Mater Phy 2020, 33 (1), 177–195. https://doi.org/10.1007/s10334-019-00790-y.

15. Bozdogan, H. Model Selection and Akaike's Information Criterion (AIC): The General Theory and Its Analytical Extensions. Psychometrika 1987, 52 (3), 345–370. https://doi.org/10.1007/BF02294361.

16. R Core Team (2022). R: A Language and Environment for Statistical Computing. https://www.R-project.org/.

17. Koo, T. K.; Li, M. Y. A Guideline of Selecting and Reporting Intraclass Correlation Coefficients for Reliability Research. Journal of Chiropractic Medicine 2016, 15 (2), 155–163. https://doi.org/10.1016/j.jcm.2016.02.012.

Figures and Tables

Sequence details	
TE	Minimum
TR	> 2 s
FOV	384 mm^2
Pixel size	3x3 mm^2
Slice orientation	Coronal
Slice thickness	5 mm
Number of slices	13

Fitting details

Algorithm ID	Algorithm Name	Description
1	ETP_SRI_LinearFitting	Linear fit
2	IAR_LU_biexp	bi-exponential NLLS
3	IAR_LU_modified_mix	Variable projection
4	IAR_LU_modified_topopro	Variable projection
5	IAR_LU_segmented_2step	2-step segmented NLLS
6	IAR_LU_segmented_3step	3-step segmented NLLS
7	IAR_LU_subtracted	2-step segmented NLLS
8	OGC_AmsterdamUMC_Bayesian_biexp	Bayesian
9	OGC_AmsterdamUMC_biexp	LSQ fitting
10	OGC_AmsterdamUMC_biexp_segmented	segmented LSQ fitting
11	OJ_GU_seg	Segmented NLLS fitting
12	PV_MUMC_biexp	two-step (segmented) LSQ fitting
13	PvH_KB_NKI_IVIMfit	two-step segmented fit approach
14	TCML_TechnionIIT_SLS	LSQ fitting
15	TCML_TechnionIIT_lsqBOBYQA	LSQ fitting
16	TCML_TechnionIIT_lsq_sls_lm	LSQ fitting
17	TCML_TechnionIIT_lsq_sls_trf	LSQ fitting
18	TCML_TechnionIIT_lsqlm	LSQ fitting
19	TCML_TechnionIIT_lsqtrf	LSQ fitting
20	TF_reference_IVIMfit	Segmented linear fitting

TE: echo time, TR: repetition time, FOV: field of view, NLLS: non linear least squares, LSQ: linear least squares

Scan for high-resolution version

Figure 1: *Table reporting common imaging paramters across sites and fitting details such as algorithm ID and names as reported in OSIPI (https://github.com/OSIPI/TF2.4_IVIM-MRI_CodeCollection)*

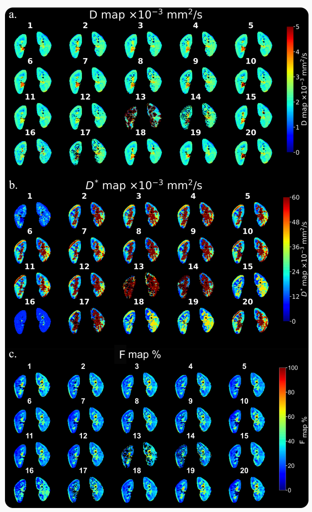

Scan for high-resolution version

Figure 2: *IVIM parameter maps from a representative volunteer: (a) D maps, (b) D* maps, and (c) F maps, showing the results from each fitting method.*

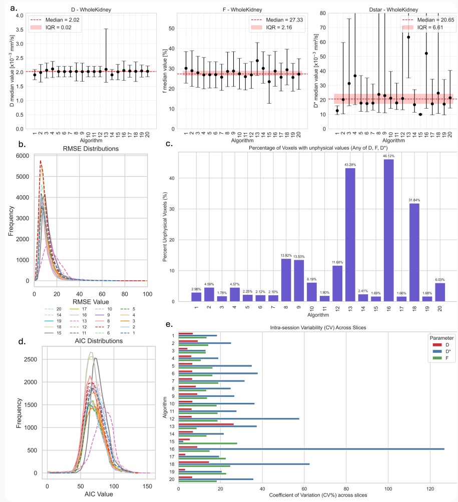

Scan for high-resolution version

Figure 3: *(a) Error bars showing the median value and interquartile range across voxels (first to third quartile) for each parameter and algorithm. The red dashed line and shaded region indicate the overall median and IQR across algorithms, respectively. (b) RMSE distributions are shown for each algorithm. (c) Percentage of unphysical values. (d) AIC distributions are shown for each algorithm. (e) Inter-slice coefficient of variation (CV%).*

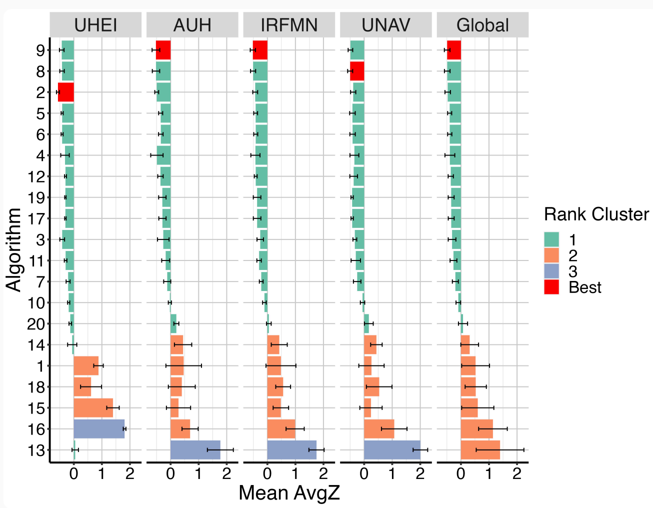

Scan for high-resolution version

Figure 4: *Average standardized z-score per algorithm across sites and globally. Bars show mean ± SD. Best-performing algorithms are highlighted in red while group color identifies average cluster rank.*

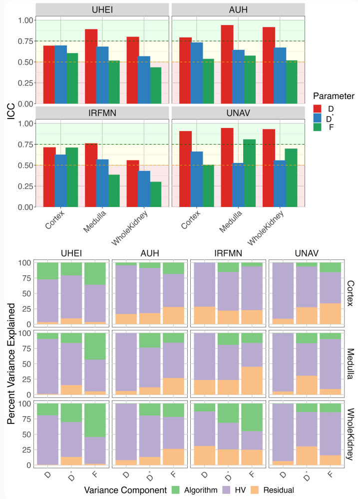

Scan for high-resolution version

Figure 5: *(a) Intraclass Correlation Coefficient (ICC) results for each parameter across regions and sites. Shaded regions indicate ICC quality: red = poor (<0.5), yellow = moderate (0.5–0.75), green = good (≥0.75). (b) Percentage of variance explained by healthy volunteer differences, algorithms, and residuals from linear mixed models for each region and parameter.*